Chemical Engineering Journal 163 (2010) 10–21

Contents lists available at ScienceDirect

Chemical Engineering Journal

journal homepage: www.elsevier.com/locate/cej

Reaction rates for supercritical water gasification of xylose in a micro-tubular reactor

Aaron K. Goodwin*, Gregory L. Rorrer

Department of Chemical Engineering, Oregon State University, Corvallis, OR 97331, United States

ARTICLE INFO

Article history:
Received 18 February 2010
Received in revised form 1 July 2010
Accepted 5 July 2010

Keywords:
Supercritical water
Biomass gasification
SCWG
Kinetic model
Xylose
Hemicellulose
Thermodynamic analysis

ABSTRACT

Two kinetic models describing supercritical water gasification of xylose at reaction temperatures from 450 °C to 650 °C and 250 bar were developed. Reaction rate constants were non-linearly estimated from product yield vs. residence time data by sum of the least squares method. The xylose decomposition kinetic model uses a detailed reaction mechanism to predict liquid intermediate production and gasification rates, whereas the xylose gasification kinetic model uses a simplified reaction mechanism to better predict gas yield and gas composition at conditions where gasification is dominant. Both models assume the gas phase reactions are in thermodynamic equilibrium, however, the gasification kinetic model accounts for non-ideal interactions in the reacting fluid by incorporating the fugacity of the gas phase species into the model using the Peng–Robinson equation of state. Major gas products were CO_2, H_2, CH_4, CO, and C_2H_6. The highest measured concentration of liquid intermediate products were acetic and propanoic acid. Finally, an analysis of gas composition and gas yields for concentrated feed stocks is discussed based on the gasification kinetic model.

1. Introduction

Hemicellulose is an amorphous biopolymer that typically makes up 25–35% of lignocellulosic biomass. Xylan, generally the most common polymer found in herbaceous crops and hardwood hemicellulose, is a hetero-polysaccharide that consists of a homopolymeric backbone of β-(1,4) linked xylose residues [1]. Lignocellulosic biomass pretreatment processes aimed at making cellulose accessible to enzymatic hydrolysis for bio-ethanol production typically produce an aqueous stream of soluble hemicellulose and lignin as a byproduct [2,3]. The amounts of hemicellulose and lignin are dependent on the chemical composition of the biomass and type and severity of the pretreatment process [2,4]. However, solubilized C_5 sugars in the pretreatment stream, such as xylose, cannot be directly fermented to ethanol by yeast typically used in the cellulose to bio-ethanol process unless they are isomerized to xylulose [5]. In addition, chemicals used in the pretreatment process may produce toxins that inhibit fermentation or cause problems in downstream processing [5]. Alternatively, the hemicellulose rich aqueous stream can be directly reformed to H_2 and CO_2 or reacted to commodity chemicals by supercritical water (374 °C and 221 bar) [4].

Biomass gasification to H_2 gas is an alternative, renewable, and CO_2 neutral energy source, and may contribute to the increasing world energy supply. Supercritical water reforming is an excellent platform to gasify biomass. Advantages include direct processing of wet feedstocks, short residence times for complete gasification, additional hydrogen generation through reforming, and generation of a compressed product gas. Recently there have been several reviews of supercritical water gasification [6–11]. Previous studies have shown that six carbon sugars in biomass, such as glucose, fructose, and cellulose, a polymer of glucose, can be completely gasified by supercritical water to H_2 and CO_2 [12–27]. Additionally, a reaction mechanism and kinetic parameter estimates for the non-catalytic gasification of glucose by supercritical water have been proposed [28–33]. However, there are very few studies on supercritical water gasification of xylose and xylan, model compounds for hemicellulose [4,12,34]. Although the reaction mechanism and kinetics for supercritical water gasification of xylose will likely be similar to glucose, differences in decomposition chemistry may affect gasification rates due to the formation or absence of refractory liquid intermediates, and the formation or suppression of coke precursors. Previous kinetic studies for xylose degradation just above and below the critical temperature of water suggest that xylose is predominantly reacted via a retro-aldol condensation and to a much lesser extent dehydrated to furfural. The relative rates of these reactions are strongly influenced by reaction conditions [35,36]. These kinetic studies provide insight for initial xylose degradation in supercritical and near critical water, however, these studies are focused on feedstock conversion, and do not report

* Corresponding author. Tel.: +1 541 420 1843; fax: +1 541 737 4600.
E-mail address: Aarongoodwin78@yahoo.com (A.K. Goodwin).

1385-8947/$ – see front matter © 2010 Elsevier B.V. All rights reserved.
doi:10.1016/j.cej.2010.07.013

Nomenclature

a_i	Peng–Robinson attraction parameter (N m^4 mol^{-2})
A_i	dimensionless form of a
A_E	pre-exponential factor in the Arrhenius equation
b_i	Peng–Robinson repulsion parameter (m^3 mol^{-1})
B_i	dimensionless form of b
CGE	carbon gasification efficiency (moles of carbon recovered in the gas per mole of carbon in the feed)
C_i	concentration of component i at reaction T and P (mol m^{-3})
$C_{Xy,O}$	initial concentration of xylose at reaction T and P (mol m^{-3})
$C_{H_2O,O}$	initial concentration of water at reaction T and P (mol m^{-3})
E_a	activation energy (kJ mol^{-1})
k_j	rate constant of reaction j (s^{-1}) and (m^3 mol^{-1} s^{-1})
$K_{eq,i}$	equilibrium constant from reaction i
K_{ij}	binary interaction coefficient between species i and j
P	reactor pressure (bar)
P_{Ci}	critical pressure of species i (bar)
r_j	rate of reaction j (mol m^{-3} s^{-1})
R_g	universal gas constant (J mol^{-1} K^{-1})
T	reactor temperature (°C)
T_{Ci}	critical temperature of species i (°C)
V_r	reactor volume (cm^3)
X_i	mole fraction of species i
Z	compressibility factor

Greek letters

Δh_{rxn}	enthalpy of reaction (kJ mol^{-1})
α	function of the acentric factor
φ_i	fugacity coefficient of species i
ν	specific volume (m^3 mol^{-1})
ν_{Ci}	critical volume of species i (m^3 mol^{-1})
ν_o	volumetric flow rate at reactor inlet (cm^3 min^{-1})
ρ_o	fluid density at reactor inlet (g cm^{-3})
ρ_R	fluid density at reactor T and P (g cm^{-3})
τ	reactor residence time based on reactor T and P (s)
ω	acentric factor

Species

AA	acetic acid
Eth	ethane
FF	furfural
Gly	glyceraldehyde
MF	methyl formate
ML	maple lactone
PA	propanoic acid
WSHS	water soluble humic substances
Xy	xylose

gasification kinetics. Currently, there are no reported investigations that determine an overall gasification reaction mechanism and model the kinetic parameters for gasification of xylose in supercritical water at conditions where gasification is dominant.

In our previous work we showed that high rates of heat transfer, characteristic of micron sized reactor passages, may significantly intensify endothermic biomass gasification reactions in supercritical water [4,13]. For example, xylose was stoichiometrically reformed to H_2 rich gas within a 1.0 s residence time at 750 °C under isothermal continuous flow conditions in a μ-tubular reactor. Furthermore, we demonstrated that the addition of xylose to phenol in the feed accelerated the gasification rate of phenol, most likely due to a hydrogen donor effect from the rapid gasification of xylose. In order to optimize any reactive process such as the co-gasification of solubilized hemicellulose and lignin in a biomass pretreatment stream, it is essential to determine intrinsic reaction kinetics and mechanistic data for each substrate.

In the present study a reaction mechanism for the supercritical water gasification of xylose is proposed and two kinetic models were developed. The decomposition kinetic model focuses on the kinetics describing the formation and gasification of major liquid intermediate products from the decomposition of xylose by supercritical water. The gasification kinetic model assumes a simplified reaction mechanism for xylose decomposition to liquid intermediates and is focused on better predicting gas yields and gas composition. Although real biomass feed streams will likely be more complex, the two models offer different perspectives on how to approach supercritical water gasification of hemicellulose rich feed streams. The decomposition kinetic model provides greater insight for production of liquid chemicals from xylose by estimating reaction rates of several major liquid intermediates, while the gasification kinetic model better predicts gasification rates and gas composition at conditions where gasification is dominant. Kinetic parameters for both models were non-linearly estimated from product yield vs. residence time data by sum of the least squares method. An isothermal, continuous flow Hastelloy-C276 μ-tubular reactor was used to gasify xylose at 250 bar and reaction temperatures ranging from 450 °C to 650 °C.

2. Model development

2.1. Reaction mechanism

The decomposition kinetic model reaction mechanism for supercritical water gasification of xylose is presented in Fig. 1. The proposed reaction scheme does not account for all liquid intermediates and gas products generated, rather only includes intermediates and products comprising more than 1% of the total carbon in the feed, with the exception of H_2 and methyl formate. All of the identified and non-identified minor compounds were consolidated into a term called water soluble humic substances (WSHS). The identification and quantification of all the minor gas and liquid products are not practical and beyond the scope of this study.

In the proposed reaction mechanism xylose is either dehydrated to furfural, or reacted via a retro-aldol condensation to glyceraldehyde and methyl formate. Glyceraldehyde is reacted to acrylic acid which is reduced, by H_2, to propanoic acid. Methyl formate, which was not present in the measured liquid products, is assumed to react rapidly to acetic acid. Propanoic and acetic acid are stoichiometrically gasified to H_2 and CO. Decomposition of propanoic acid may also proceed down a second pathway where it is gasified to ethane and CO_2. There are three proposed pathways for the decomposition of furfural. In the first pathway, furfural is gasified directly to CO, H_2, CH_4, and CO_2. In the second pathway, furfural is reacted to maple lactone, which is gasified to CO, H_2, and CH_4. Lastly, furfural is broken down to WSHS, which is gasified to CO and H_2. Since WSHS include all of the minor liquid products, it is difficult to incorporate this term in the model. Nevertheless, the majority of the recalcitrant liquid intermediates are likely products of furfural reacted species. Finally, the water gas shift reaction and the methanation reaction were assumed to be at thermodynamic equilibrium based on the ideal gas law.

The gasification kinetic model reaction mechanism is a simplified version of the previous reaction mechanism, and is presented in Fig. 2. This reaction mechanism assumes that xylose is either dehydrated to furfural or decomposed to WSHS. Additionally, fur-

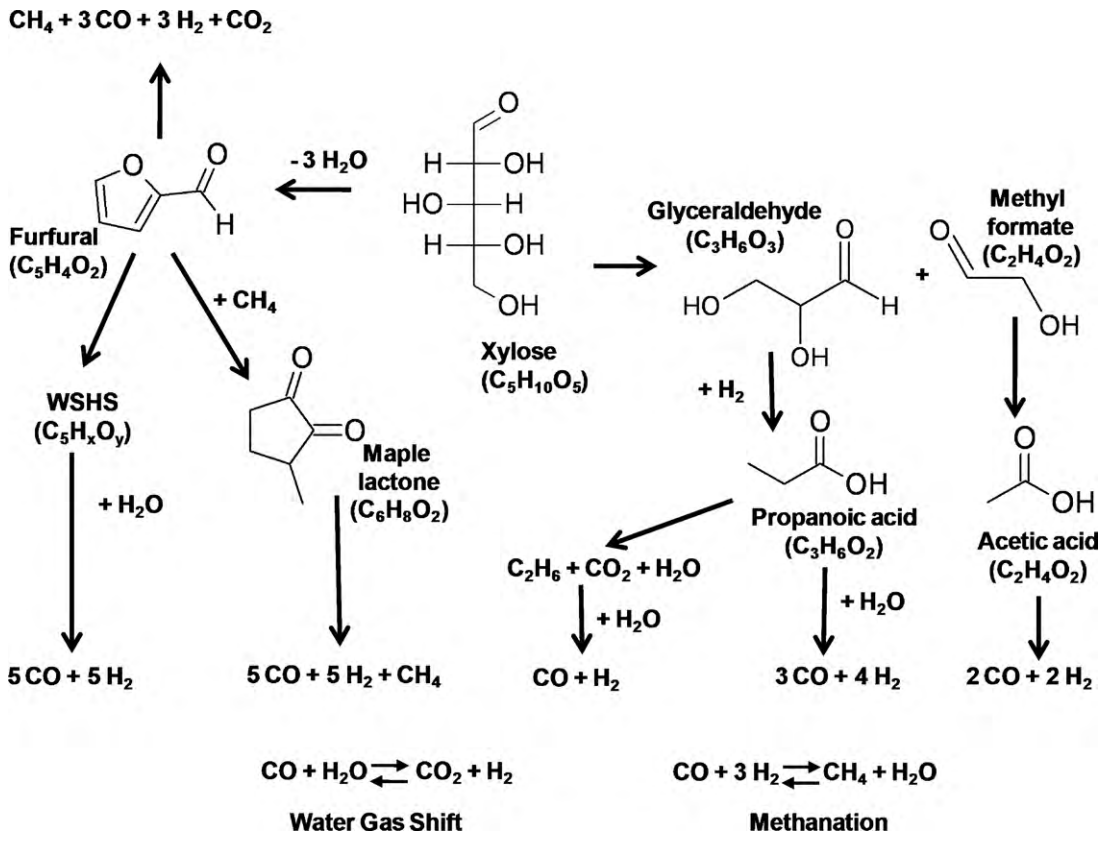

Fig. 1. Proposed decomposition kinetic model reaction mechanism for gasification of xylose by supercritical water.

fural is reacted to WSHS, and WSHS is gasified to CO and H_2. The water gas shift and methanation reactions are assumed to be in thermodynamic equilibrium, as in the previous model however, the non-ideal behavior of each species in the reacting fluid is accounted for by incorporating the fugacity coefficient of each species based on the Peng–Robinson equation of state into the model.

2.2. Rate equations and kinetic parameter estimates

The development of both kinetic models was governed by four major assumptions. The first assumption was an isothermal reacting fluid. This assumption was based on heat transfer calculations and reactor design described in our previous work [4]. Second, in the decomposition kinetic model the concentration of water is constant and calculated at the temperature and pressure of the reactor. The concentration of water was used to calculate equilibrium values for the water gas shift and methanation reaction. In all other reactions that consumed water, the concentration was included in the rate constant, and the reaction was assumed to be pseudo first order. The gasification kinetic model assumed a non-constant concentration of water, initially calculated at the temperature and pressure of the reaction. Third, all of the liquid decomposition and gasification reactions are irreversible and first order or pseudo first order with respect to the reactants. All of the gas phase reactions were reversible and assumed to be at thermodynamic equilibrium. Equilibrium relationships for the water gas shift and methanation reactions in the vapor phase as a function of temperature were obtained from *Chemcad 6* (Chemstations Inc.). Fourth, the temperature dependence of the rate constants can be described by the Arrhenius equation. Based on the previous assumptions the decomposition, gasification, and gas phase reactions and their rates for the decomposition kinetic model are as follows:

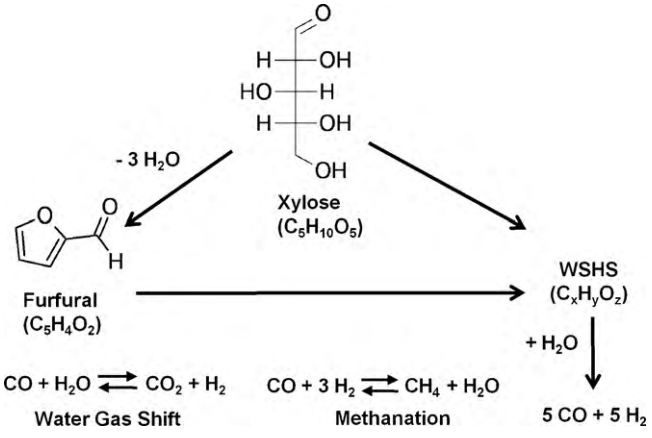

Fig. 2. Proposed simplified gasification kinetic model reaction mechanism for gasification of xylose by supercritical water.

$$C_5H_{10}O_5(Xy) \xrightarrow{k_1} C_2H_4O_2(MF) + C_3H_6O_3(Gly) \qquad r_1 = k_1 C_{Xy} \tag{1}$$

$$C_5H_{10}O_5(Xy) \xrightarrow{k_2} C_5H_4O_2(FF) + 3H_2O \qquad r_2 = k_2 C_{Xy} \tag{2}$$

$$C_3H_6O_3(Gly) + H_2 \xrightarrow{k_3} C_3H_6O_2(PA) + H_2O \qquad r_3 = k_3 C_{Gly} C_{H_2} \tag{3}$$

$$C_2H_4O_2(MF) \xrightarrow{k_4} C_2H_4O_2(AA) \qquad r_4 = k_4 C_{MF} \tag{4}$$

$$C_5H_4O_2(FF) \xrightarrow{k_5} C_xH_yO_z(WSHS) \qquad r_5 = k_5 C_{WSHS} \tag{5}$$

$$C_5H_4O_2(FF) + CH_4 \xrightarrow{k_6} C_6H_8O_2(ML) \qquad r_6 = k_6 C_{FF} C_{CH_4} \tag{6}$$

$$C_3H_6O_3(PA) + H_2 \xrightarrow{k_7} C_2H_6 + H_2O + CO_2 \qquad r_7 = k_7 C_{PA} C_{H_2} \tag{7}$$

$$C_2H_4O_2(AA) \xrightarrow{k_8} 2CO + 2H_2 \qquad r_8 = k_8 C_{Eth} \tag{8}$$

$$C_3H_6O_2(PA) + H_2O \xrightarrow{k_9} 3CO + 4H_2 \qquad r_9 = k_9 C_{PA} \tag{9}$$

$$C_5H_4O_2(FF) + 3H_2O \xrightarrow{k_{10}} CO_2 + CH_4 + 3CO + 3H_2 \qquad r_{10} = k_{10} C_{FF} \tag{10}$$

$$C_xH_yO_z(WSHS) + wH_2O \xrightarrow{k_{11}} 5CO + 5H_2 \qquad r_{11} = k_{11} C_{WSHS} \tag{11}$$

$$C_6H_8O_2(ML) + 3H_2O \xrightarrow{k_{12}} CH_4 + 5CO + 5H_2 \qquad r_{12} = k_{12} C_{ML} \tag{12}$$

$$C_2H_6 + H_2O \xrightarrow{k_{13}} 2CO + 5H_2 \qquad r_{13} = k_{13} C_{Eth} \tag{13}$$

$$CO + H_2O \underset{k_{15}}{\overset{k_{14}}{\rightleftarrows}} H_2 + CO_2 \qquad r_{14} = k_{14} C_{CO} C_{H_2O} - k_{15} C_{H_2} C_{CO_2} \tag{14}$$

$$CO + 3H_2 \underset{k_{17}}{\overset{k_{16}}{\rightleftarrows}} CH_4 + H_2O \qquad r_{15} = k_{16} C_{CO} C_{H_2}^3 - k_{17} C_{CH_4} C_{H_2O} \tag{15}$$

The concentration of each component '*i*' (C_i) as a function of time can be expressed in terms of the following differential equations for each of the 13 species:

$$\frac{dC_{Xy}}{dt} = -r_1 - r_2 \tag{16}$$

$$\frac{dC_{Gly}}{dt} = r_1 - r_3 \tag{17}$$

$$\frac{dC_{MF}}{dt} = r_1 - r_4 \tag{18}$$

$$\frac{dC_{AA}}{dt} = r_4 - r_8 \tag{19}$$

$$\frac{dC_{PA}}{dt} = r_3 - r_7 \tag{20}$$

$$\frac{dC_{FF}}{dt} = r_2 - r_5 - r_6 - r_{10} \tag{21}$$

$$\frac{dC_{ML}}{dt} = r_6 - r_{12} \tag{22}$$

$$\frac{dC_{WSHS}}{dt} = r_5 - r_{11} \tag{23}$$

$$\frac{dC_{Eth}}{dt} = r_7 - r_{13} \tag{24}$$

$$\frac{dC_{CO_2}}{dt} = r_7 + r_{10} + r_{14} \tag{25}$$

$$\frac{dC_{CO}}{dt} = 2r_8 + 3r_9 + 3r_{10} + 5r_{11} + 5r_{12} + 2r_{13} - r_{14} - r_{15} \tag{26}$$

$$\frac{dC_{CH_4}}{dt} = r_{12} + r_{15} + r_{11} - r_6 \tag{27}$$

$$\frac{dC_{H_2}}{dt} = 2r_8 + 4r_9 + 3r_{10} + 5r_{11} + 5r_{12} + 5r_{13} + r_{14} - 3r_{15} - r_7 - r_3 \tag{28}$$

Reaction and rate equations for the gasification kinetic model are:

$$C_5H_{10}O_5(Xy) \xrightarrow{k_{18}} C_5H_4O_2(FF) + 3H_2O \qquad r_{18} = k_{18} C_{Xy} \tag{29}$$

$$C_5H_{10}O_5(Xy) \xrightarrow{k_{19}} C_xH_yO_z\,(WSHS) \qquad r_{19} = k_{19} C_{Xy} \tag{30}$$

$$C_5H_4O_2(FF) \xrightarrow{k_{20}} C_xH_yO_z(WSHS) \qquad r_{20} = k_{20} C_{FF} \tag{31}$$

$$C_xH_yO_z(WSHS) \xrightarrow{k_{21}} 5CO + 5H_2 \qquad r_{21} = k_{21} C_{WSHS} \tag{32}$$

The water gas shift, Eq. (14), and the methanation reaction, Eq. (15), are included in the gasification model. The differential equations that describe the gasification kinetic model are

$$\frac{dC_{Xy}}{dt} = -r_{18} - r_{19} \tag{33}$$

$$\frac{dC_{FF}}{dt} = r_{18} - r_{20} \tag{34}$$

$$\frac{dC_{WSHS}}{dt} = r_{19} + r_{20} - r_{21} \tag{35}$$

$$\frac{dC_{CO}}{dt} = 5r_{21} - r_{14} - r_{15} \tag{36}$$

$$\frac{dC_{H_2}}{dt} = 5r_{21} + r_{14} - 3r_{15} \tag{37}$$

$$\frac{dC_{CO_2}}{dt} = r_{14} \tag{38}$$

$$\frac{dC_{CH_4}}{dt} = r_{15} \tag{39}$$

$$\frac{dC_{H_2O}}{dt} = r_{14} - r_{15} \tag{40}$$

The initial conditions at $t = 0$ for the differential equations for both models are $C_{Xy} = C_{Xy,O}$; $C_{H_2O} = C_{H_2O,O}$; $C_{Gly} = C_{MF} = C_{AA} = C_{PA} = C_{FF} = C_{ML} = C_{WSHS} = C_{Eth} = C_{CO_2} = C_{CO} = C_{CH_4} = C_{H_2} = 0$. Concentration values for all species are in moles m^{-3} at the temperature and pressure of the reaction. Carbon gasification efficiency (CGE) was based on the percentage of recovered carbon in the gas from the feed

$$CGE = \frac{\sum_{i,g} n_i C_{i,g}(T,P)}{n_{Xy} C_{Xy,o}(T,P)} \tag{41}$$

where n is the moles of carbon per mole of species, and $C_{i,g}$ are the concentration of the gas phase species, CO_2, CO, CH_4, C_2H_6, C_2H_4, C_2H_2 at reactor temperature and pressure. Hydrogen yield was defined as the amount of H_2 produced per mole of xylose reacted. Product gas composition was calculated by

$$X_i = \frac{C_i(T,P)}{\sum_{i,g} C_{i,g}(T,P)} \tag{42}$$

where X_i is the mole fraction of component i. Water was not included in the product gas composition. Thermodynamic equilibrium rate constants for gas phase reactions were calculated by the van't Hoff equation assuming a constant Δh°_{rxn}. Fugacity coefficients for each species in the mixture were calculated from the Peng–Robinson equation of state to account for non-ideal gas behavior of each species in the reacting fluid.

$$P = \frac{R_g T}{v - b} - \frac{a\alpha}{v(v+b) + b(v-b)} \tag{44}$$

where a and b are interaction parameters given by

$$a_i = \frac{0.457 R_g^2 T_c^2}{P_c} \tag{45}$$

$$b_i = \frac{0.0778 R_g T_c}{P_c} \tag{46}$$

and α is a function of the acentric factor given by

$$\alpha = \left(1 + \left(0.37464 + 1.54266\omega - 0.266992\omega^2\right)\left(1 - \left(\frac{T}{T_c}\right)^{0.5}\right)\right)^2 \tag{47}$$

where ω is the acentric factor for each pure species i. This equation of state is appropriate for thermodynamic analysis of supercritical fluid applications including supercritical water gasification [37]. van der Waals mixing rules were used to apply the Peng–Robinson equation to a mixture

$$a = \sum_i^n \sum_j^n X_i X_j a_{ij} \tag{48}$$

$$b = \sum_{i}^{n}\sum_{j}^{n} X_i X_j b_{ij} \tag{49}$$

$$a_{ij} = \left(1 - k_{ij}\right)\left(a_i - a_j\right)^{0.5} \tag{50}$$

$$b_{ij} = \frac{\left(b_i + b_j\right)}{2} \tag{51}$$

where k_{ij} is an additional interaction parameter estimated by

$$k_{ij} = 1 - \frac{8\left(v_{ci}v_{cj}\right)^{0.5}}{\left(v_{ci}^{1/3} + v_{cj}^{1/3}\right)^{3}} \tag{52}$$

Based on the Peng–Robinson equation of state, the compressibility factor, Z, and the Van der Waals mixing rules the fugacity coefficient for each component in the mixture could be calculated by

$$\ln\phi_i = \frac{B_i}{B}(Z-1) - \ln(Z-B) - \frac{A}{2(2B)^{0.5}}\left(\frac{2\sum_j X_i A_{ij}}{A} - \frac{B_i}{B}\right) \ln\left(\frac{Z + \left(1+\sqrt{2}\right)B}{Z + \left(1-\sqrt{2}\right)B}\right) \tag{53}$$

The dimensionless interaction and repulsion parameters A and B are given by

$$A_i = \frac{a_i P}{\left(R_g T\right)^2} \tag{54}$$

$$B_i = \frac{b_i P}{RT} \tag{55}$$

Fugacity coefficients were used in the gasification kinetic model to more accurately calculate equilibrium gas phase concentrations for CO, CO_2, CH_4, H_2, and H_2O in Eqs. (14) and (15). Easy Fit Model Design version 4.32 was used to non-linearly fit rate constants to the set of differential Eqs. (16)–(28) and (33)–(40) at 450 °C, 500 °C, and 550 °C. Parameters for the rate constant estimation are presented in Table 1. All data points were equally weighted, and initial guesses for the rate constants were determined by trial and error method.

Table 1
Summary of rate constant fitting parameters.

Decomposition kinetic model	
Number of differential Equations	13
Number of measurements sets	13
Confidence level	95%
Initial step size	0.001
Gradient evaluation	Two sided difference
Termination tolerance	1.00E−09
Final residual estimate	1.00E−06
Error estimation	Sum of the squared Residuals
Residence time range for fitted Experimental data	3.0–24.0 s (450 °C) 2.5-16.4 s (500 °C) 1.1–8.6 s (550 °C)
Gasification kinetic model	
Number of differential Equations	7
Number of measurements sets	7
Confidence level	95%
Initial step size	0.001
Gradient evaluation	Two sided difference
Termination tolerance	1.00E−09
Final residual estimate	1.00E−06
Error estimation	Sum of the squared Residuals
Residence time range for fitted Experimental data	3.0–40.0 s (450 °C) 2.5–24.6 s (500 °C) 1.1–21.5 s (550 °C)

3. Experimental

3.1. Micro-tubular reactor and test loop

A 2 m long, 1.6 mm (1/16 in.) outer diameter, 762 μm (0.03 in.) inner diameter Hastelloy-C-276 tube with a volume of 0.912 cm^3 (VICI THC-130) served as the μ-tubular reactor (Fig. 1a). The tube was inserted into a milled stainless steel reactor block. Details of the reactor setup have been previously described [4].

The continuous flow reactor test loop is presented in Fig. 3. The feed was pumped to the reactor, at 25 °C and 250 bar, by a Teledyne Isco 260D syringe pump (266 ml capacity) operating at constant flow. The feed was heated and maintained at the reaction temperature by two 375 W flat plate ceramic heaters (Thermcraft Inc., 29.5 cm × 7.93 cm × 2.06 cm with a Ni–Cr wire heating element) that were mounted to the top and bottom of the reactor heating block. The reactor temperature was maintained by a PID controller with a Type J thermocouple inserted into the center of the reactor heating block. All sides of the reactor heating block were insulated with 3.8 cm thick Fibercraft board (Thermcraft, Inc.). Due to the narrow bore of the tubing it was not possible to directly measure the reacting fluid temperature, however previous calculations suggest the reactor temperature is isothermal [4].

The hot reactor effluent exiting the reactor was cooled to 20 °C with a shell and tube heat exchanger using water as the coolant. The pressure was decreased from 250 bar to 1.03 bar by an adjustable precision back-pressure regulator (KHB1WOA6C2P6000, Swagelok Inc., stainless steel). The condensed liquid products were collected for further analysis. The gas products were dried and quantified with a gas mass flowmeter (Omega Inc. FMA 1800 series, 0–20 sccm, and 0–100 sccm, aluminum/brass body). Gas samples were collected in a 2.0 L Tedlar gas collection bag and corrected for gas composition.

The feed solution consisted of 4.0 wt% α-D-xylose (Sigma–Aldrich X1500, >99% purity, CAS108-95-2, molecular weight 150.13) dissolved in 96 wt% de-ionized distilled water. All xylose feed solutions were degassed with helium prior to use. The liquid feed flow rate to the reactor ranged from 0.15 ml/min to 8.0 ml/min at 25 °C and 250 bar. The fluid residence time (τ) was estimated by $\tau = V_R\rho_R/v_o\rho_o$. Where V_R is the reactor volume (cm^3), v_o is the volumetric flowrate ($cm^3\,min^{-1}$) of the liquid feed at the reactor inlet temperature T_o, and system pressure P, ρ_o is the density of the liquid feed at T_o and P ($g\,cm^{-3}$), and ρ_R is the density of the fluid at the reactor set point temperature T and P ($g\,cm^{-3}$). The reactor residence time is based on the fluid properties at the reactor set point temperature and pressure, and does not account for fluid density changes as the fluid heats up from the subcritical liquid state to the supercritical fluid state. The fluid physical properties were estimated from water at the reactor temperature and pressure. Therefore, density or heat effects from the formation of gas products in the reactor were not factored into the residence time calculation. Newly installed Hastelloy-C-276 microtubes were conditioned as previously reported [4].

3.2. Analytical procedures

Gas and liquid products were analyzed by gas chromatography (GC) and high performance liquid chromatography (HPLC). Gas products were quantitatively analyzed by a SRI multiple gas analyzer #1 equipped with a thermal conductivity detector for H_2 analysis, and a FID detector with a methanizer for CO, CH_4, CO_2, C_2H_2, C_2H_4, and C_2H_6 analysis. The gas mixture was separated on

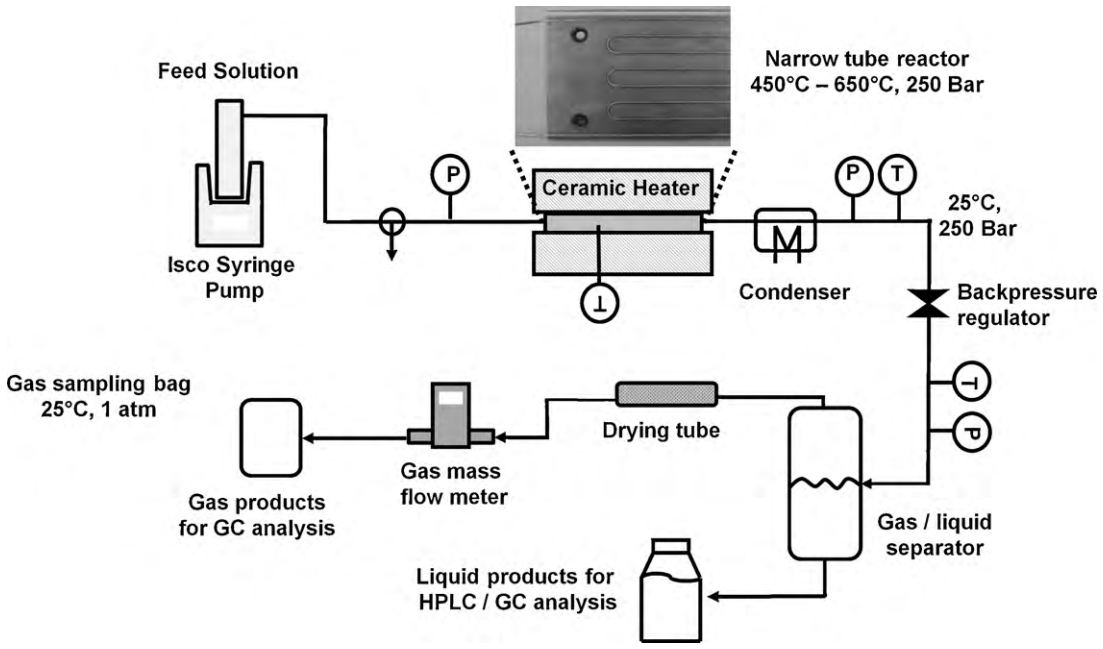

Fig. 3. Continuous flow micro-tubular reactor test loop.

two columns, a 2-m Molecular Sieve 13X and a 2-m silica gel. The GC oven temperature was held at 40 °C for 3 min, then ramped to 135 °C at a rate of 16 °C/min, and finally held at 135 °C for 2.67 min. A standard gas injection volume of 250 μl was injected three times for all gas samples. The concentration of the gas species was reported as an average of three injections, and the standard deviation was typically less than 2% of the reported value. Gas products were identified by retention time and quantified by external calibration against a standard gas mixture (Alltech Associates Inc., gas standard #19792). Calibration was performed with three 100 μl standard gas injections. Procedures for the analysis of residual sugar, organic acids, and other organic liquid intermediates present in the liquid products by high performance liquid chromatography (HPLC) were previously described [4]. For liquid products measured by HPLC an average peak area of two injections was reported, and the standard error was less typically than 10%.

4. Results and discussion

Two kinetic models were developed to describe intrinsic reaction kinetics for supercritical water gasification of xylose. The decomposition model focuses on estimating kinetic parameters for major liquid intermediates governed by the reaction mechanism in Fig. 1. By using a simplified reaction mechanism, presented in Fig. 2, the gasification kinetic model primarily focuses on predicting gas composition, H_2 yield, and gasification rates at conditions where gasification is dominant. Both models assume the water gas shift and methanation reactions are in thermodynamic equilibrium, however, the gasification kinetic model compensates for the non-ideal behavior of the gas species by accounting for the species fugacity in the mixture derived from the Peng–Robinson equation of state and van der Waals mixing rules. Additionally, water is incorporated into the model as a reacting species to better predict gas composition for high feed stock concentrations. For dilute feedstock concentrations these reactions are dominated by the law of mass action due to the large concentration of water present in the reacting fluid.

The decomposition kinetic model is more appropriate for predicting and investigating the synthesis of commodity chemicals derived from supercritical water reforming of hemicellulose rich feed streams, whereas the gasification model is appropriate for modeling and optimization for gasification of hemicellulose rich feed streams. Kinetic parameter estimations and their errors for Eqs. (1)–(13) and (29)–(32) are presented in Table 2. The somewhat large error associated with the estimated kinetic terms is most likely due to an incomplete reaction mechanism rather than poor data.

4.1. Liquid phase analysis

The decomposition kinetic model will primarily be used to analyze the liquid products for supercritical water gasification of xylose. Major liquid intermediates from the supercritical water gasification of xylose are all water soluble and can be found in Fig. 1. Given that complete conversion of xylose was achieved at all temperatures and residence times tested, it is useful to compare

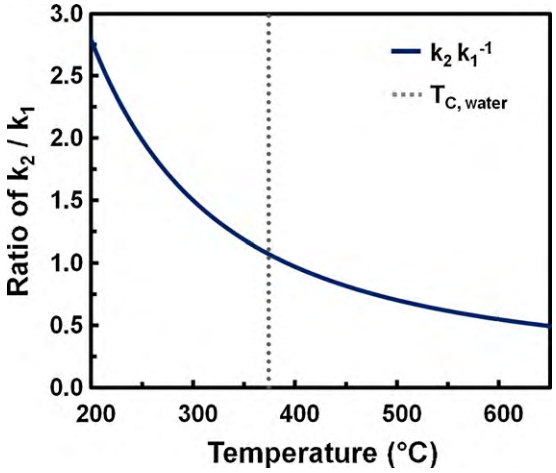

Fig. 4. Ratio of rate constants k_1/k_2 from the decomposition kinetic model. Estimated reaction rate k_1 is the decomposition of xylose to furfural, and k_2 is the decomposition of xylose to glyceraldehyde and methyl formate. The vertical dashed line represents the critical temperature of water.

Table 2
Summary of estimated kinetic parameters. *Due to an estimated rate constant of 0 s^{-1} at 450 °C, k_{10} was estimated by plotting the estimated rate constants at 500 °C and 550 °C vs. temperature and estimating the activation energy and pre-exponential.

Rate constant	Activation energy		Pre-exponential		
	(kJ mol^{-1})	Error (±)	(s^{-1})	Error (+)	Error (−)
Decomposition kinetic model					
k_1	134.0	19.5	1.5E+13	3.1E+14	7.0E+11
k_2	120.1	11.1	1.2E+12	6.6E+12	2.1E+11
k_3	43.9	0.1	9.5E+04	9.7E+04	9.3E+04
k_4	250.7	3.8	7.5E+23	1.4E+24	4.2E+23
k_5	55.6	34.9	5.7E+03	1.3E+06	2.4E+01
k_6	532.4	313.7	4.4E+35	8.6E+56	2.3E+14
k_7	80.6	41.9	3.3E+03	2.3E+06	4.8E+00
k_8	81.5	37.6	1.0E+05	3.6E+07	2.9E+02
k_9	89.4	55.2	1.4E+05	7.9E+08	2.5E+01
k_{10}*	157.3	N/A	1.0E+09	N/A	N/A
k_{11}	138.9	10.9	1.6E+08	8.5E+08	2.8E+07
k_{12}	161.7	16.7	3.5E+10	4.8E+11	2.6E+09
k_{13}	0.0	0.0	0.0E+00	0.0E+00	0.0E+00
Gasification kinetic model			I		
k_{18}	147.5	3.8	1.3E+13	2.4E+13	7.1E+12
k_{19}	154.7	9.4	6.6E+14	2.8E+15	1.5E+14
k_{20}	100.5	0.5	1.7E+06	1.8E+06	1.5E+06
k_{21}	142.7	1.5	3.5E+08	4.5E+08	2.8E+08

kinetic parameter estimates to published values. The activation energy and pre-exponential term for the dehydration of xylose to furfural in the decomposition model, Eq. (2), were estimated to be 120 kJ mol^{-1}, and 1.2 × 10^{12} s^{-1} respectively, and 147.5 kJ mol^{-1} and 1.3 × 10^{13} s^{-1} for the gasification model, Eq. (29). Both values are in good agreement with Qi and Xiuyang [35] who estimated the activation energy to be 111 kJ mol^{-1}, and pre-exponential of 1.4 × 10^{12} s^{-1} for dehydration of xylose to furfural in near critical water. Activation energy and pre-exponential for xylose degradation by retro-aldol condensation to glyceraldehyde and methyl formate were estimated to be 134 kJ mol^{-1}, and 1.5 × 10^{13} s^{-1} in the decomposition model, and were higher than previous published values of 102 kJ mol^{-1} and 6.9 × 10^{8} reported by Sasaki et al. [36]. The difference may be attributed to the reactor material. Whereas this study uses Hastelloy-C-276, Sasaki et al. [36] used stainless steel reactor tubing. Nickel, which makes up a significant larger percentage of the Hastelloy-C-276 than stainless steel, has been shown to catalyze gasification reactions of glucose and cellulose [19,26]. It is likely that nickel in the reactor wall will have a similar catalytic effect for xylose decomposition in supercritical water. The

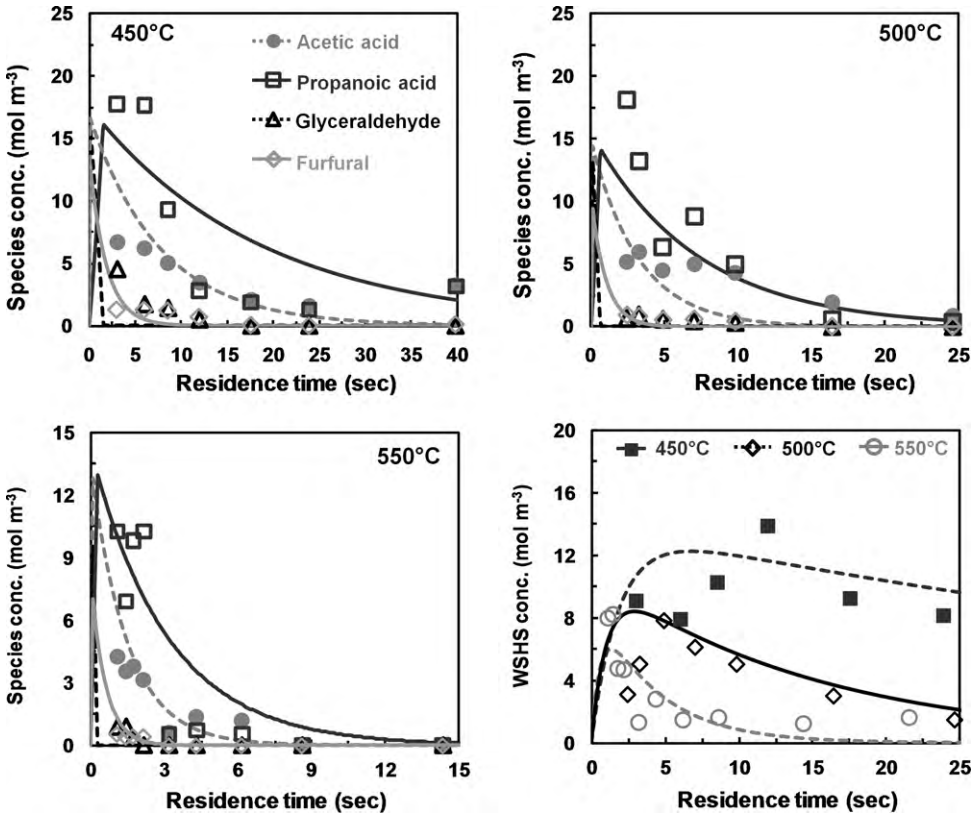

Fig. 5. Liquid phase intermediate product formation from the supercritical water gasification of xylose (4.0 wt%, 277 mM) vs. residence time at 450 °C, 500 °C, 550 °C, and 650 °C. The solid and dashed lines represent the non-linear least squares fit of the data to the decomposition kinetic model.

calculated ratio of the rate constants (k_2/k_1) for the decomposition model is plotted vs. temperature and is presented in Fig. 4. The ratio of the rate constants is unity just above the critical temperature for water, which suggests that xylose dehydration to furfural is favored below the critical temperature of water in an ionic reaction environment, while retro-aldol condensation to pyruvaldehyde and methyl formate is favored above the critical point of water in a free radical dominated reaction environment. This is consistent with previous mechanistic studies for xylose and glucose in near and supercritical water [28,33,36]. Given that the mechanism for xylose decomposition changes from ionic to free radical at the critical temperature of water, rate constants for xylose dehydration to furfural and retro-aldol condensation to pyruvaldehyde and methyl formate can significantly affect gas and liquid product yield prediction at temperatures just above the critical temperature of water. Of the two reaction mechanisms described, the decomposition reaction mechanism can more accurately predict gas and liquid product yields for xylose gasification just above the critical temperature of water.

Since the term WSHS in the decomposition model is based on the formation and gasification of minor liquid products derived from furfural, it is useful to compare the estimated kinetic parameters to literature values. Consequently, Qi and Xiuyang [35] estimated the rate constant for the reaction of furfural to "decomposition products" just below the critical point of water. Although the reaction mechanisms for both models differ slightly and Qi and Xiuyang [35] study was focused on feedstock conversion and not gasification, estimates for the activation energy and pre-exponential term, 58.8 kJ mol^{-1} and 2.0×10^3 s^{-1}, were in good agreement with our estimates of 55.6 kJ mol^{-1} and 5.7×10^3 s^{-1}.

The rate constant for the reaction of ethane to CO and H_2, Eq. (13) in the decomposition model, was estimated to be zero at 450 °C, 500 °C, and 550 °C indicating the concentration of ethane has reached a pseudo steady state, and was not being further reacted to CO and H_2. Additionally, due to an estimated value of zero at 450 °C and higher values at 500 °C and 550 °C, the activation energy for the rate constant k_{10}, Eq. (10), was determined by estimating the pre-exponential of the Arrhenius equation based on similar reactions, and minimizing the sum of the squares of the error between the estimated rate constants and the Arrhenius equation to determine the activation energy. The activation energy was estimated to be 157.3 kJ mol^{-1}.

Selected concentrations of liquid intermediates generated during xylose gasification by supercritical water vs. reactor residence time are presented in Fig. 5. The solid and dashed lines represent fits from the decomposition kinetic model. Major refractory liquid intermediates were acetic acid, propanoic acid, furfural, and glyceraldehyde. The measured concentration of the major refractory intermediates decreased with increasing residence times. Of the major liquid intermediates, acetic acid and propanoic acid had the highest predicted and measured concentration. Other modeled liquid products were xylose, maple lactone, and methyl formate. Methyl formate and xylose had a zero measured concentration for all conditions tested, indicating that complete xylose conversion was achieved, and the conversion of methyl formate to acetic acid is very rapid. The highest concentration of maple lactone was 0.17 mol m^{-3} at 450 °C and 8.6 s residence time, and accounted for 1.0% of the total carbon in the feed. Although there is no proposed reaction pathway for the production of maple lactone from furfural, Williams and Onwudili [31] proposed a reaction pathway for the formation of 3-methyly cyclopenten-2-one from 5-hydroxymethyl-furfural (5-HMF). It is likely that maple lactone is derived by a similar reaction pathway, and is a product of furfural and an unknown minor intermediate. In our proposed reaction mechanism furfural reacts with CH_4 to form maple lactone. Although the reaction mechanism is likely more complicated, this simplified reaction pathway is sufficient to preserve the carbon balance.

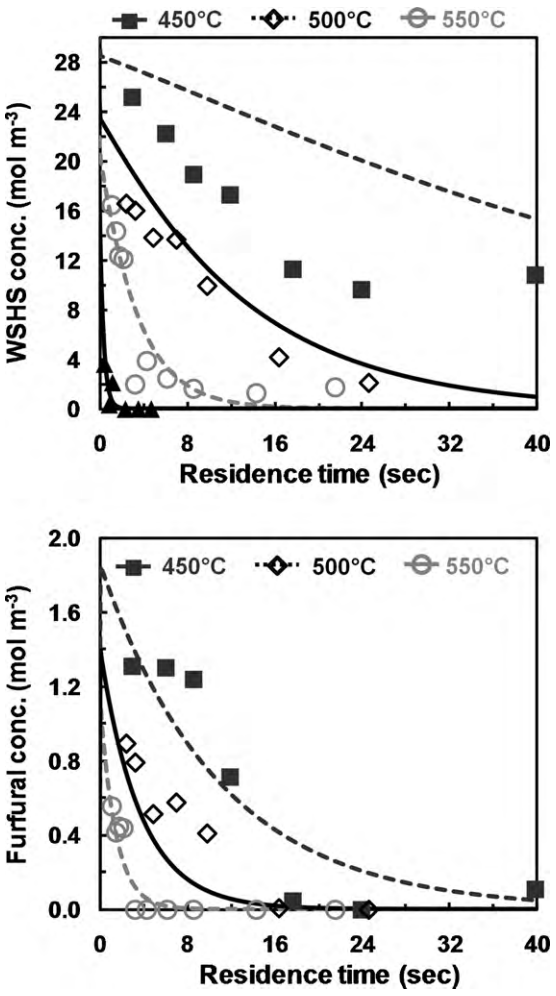

Fig. 6. Liquid phase concentration of WSHS and furfural at 450 °C, 500 °C and 550 °C. The solid and dashed lines represent the non-linear least squares fit of the data to the gasification kinetic model.

The remainder of the unaccounted for minor intermediate products based on carbon in the liquid products was lumped into WSHS and accounted for up to 34% of the total carbon in the feed. The effect of residence time on the concentration of WSHS at 450 °C, 500 °C and 550 °C is presented in Fig. 5. Generally, the concentration of WSHS increased to a maximum, leveled off, and decreased with increasing residence time. The concentration of WSHS was greatest at 450 °C and a 12 s residence time, and decreased with increasing temperature. There was no WSHS at 650 °C at the majority of residence times tested due to complete gasification of the feedstock. No carbon formation or reactor plugging was observed in any of the experiments, and thus was not integrated into either kinetic model.

The approach used to account for liquid phase intermediates in the gasification kinetic model was to assume that xylose was either dehydrated to furfural or reacted to WSHS. The term WSHS in this model accounted for all major and minor liquid intermediates other than furfural. Concentrations of WSHS and furfural as a function of residence time and temperatures are presented in Fig. 6. The concentration of WSHS and furfural decreased with increasing residence time, and the rate both species reacted increased with reaction temperature. These results are indicative of an Arrhenius relationship between reaction temperature and reaction rate. The gasification kinetic model fit the data well except at a reac-

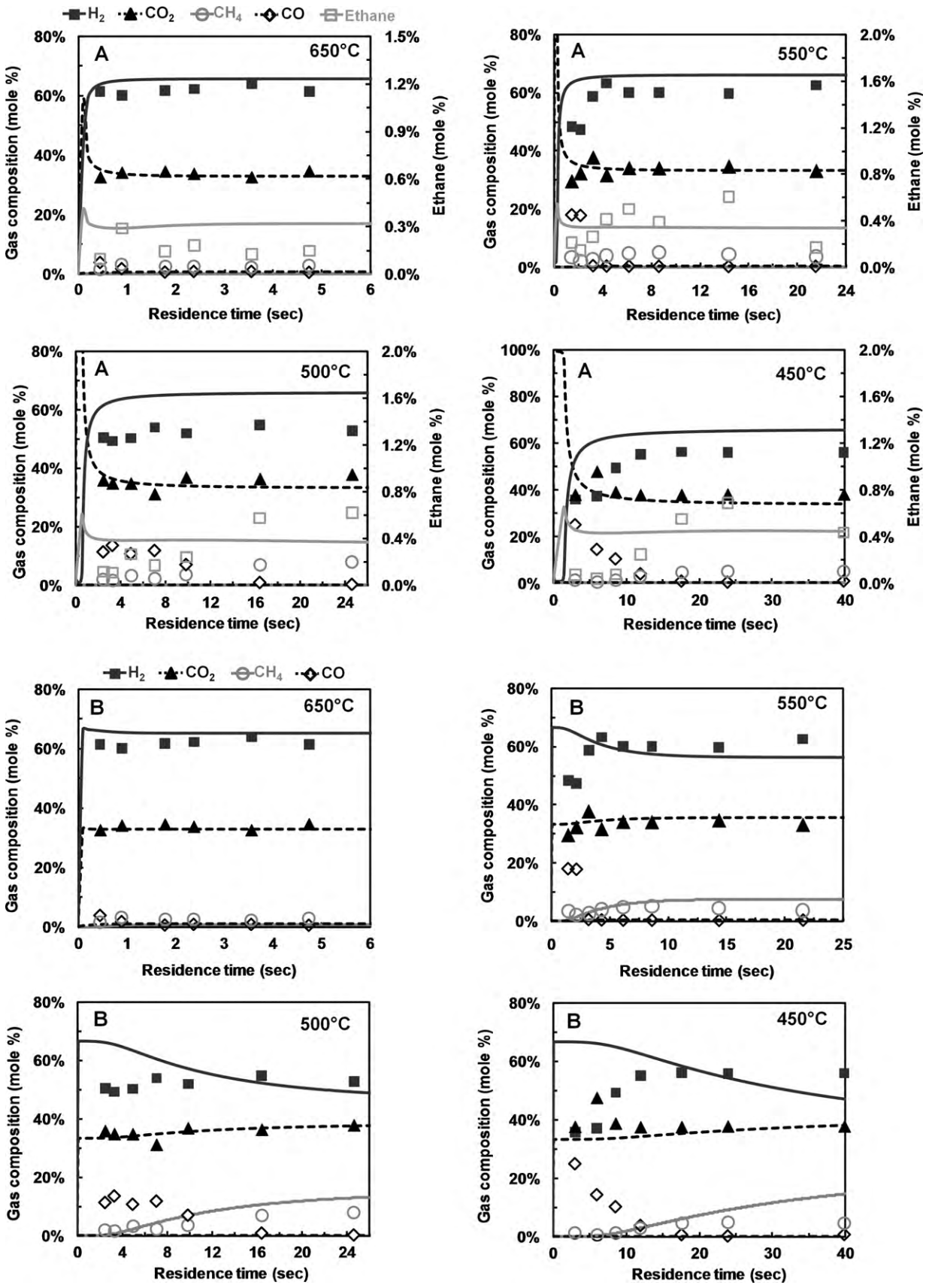

Fig. 7. Gas composition from the supercritical water gasification of xylose (4.0 wt%, 277 mM) vs. residence time at 450 °C, 500 °C, 550 °C, and 650 °C. The solid and dashed lines represent the non-linear least squares fit of the data to the (A) decomposition kinetic model and (B) gasification kinetic model.

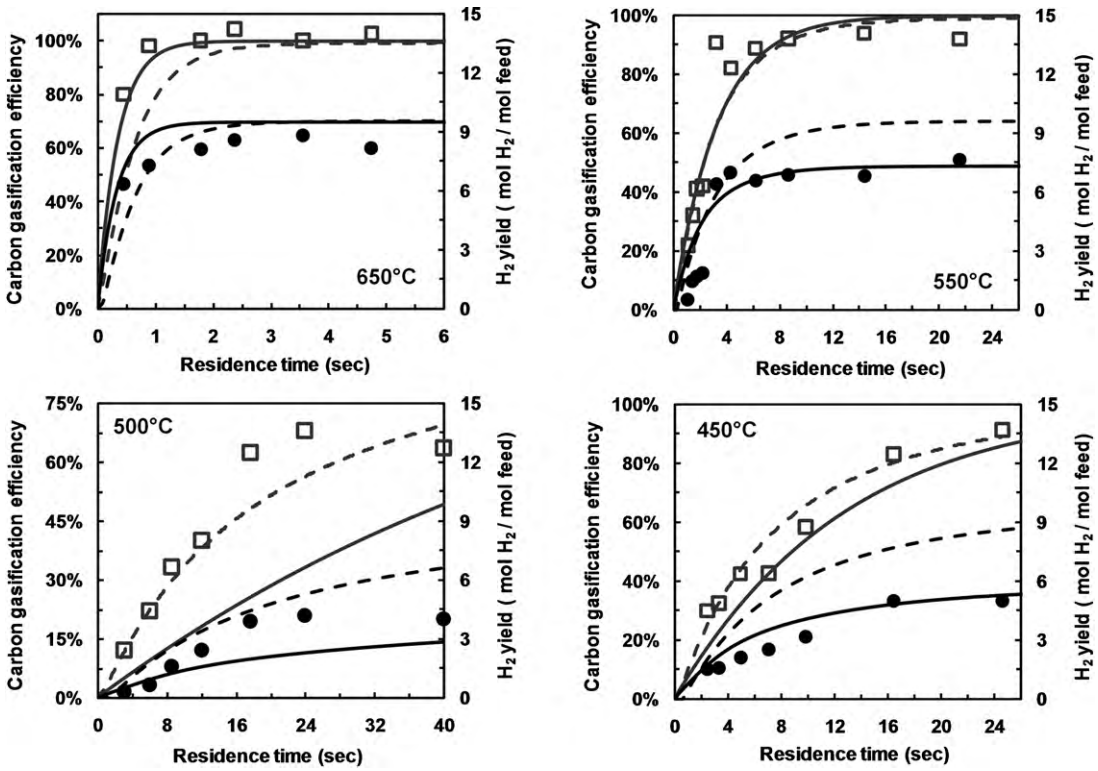

Fig. 8. Carbon gasification efficiency and H_2 yield from the supercritical water gasification of xylose (4.0 wt%, 277 mM) vs. residence time at 450 °C, 500 °C, 550 °C, and 650 °C. The solid lines are fits from the gasification model and dashed lines are fits from the decomposition kinetic model.

tion temperature of 450 °C when the model over predicted the concentration of WSHS. The over prediction was most likely due to constrained rate constant estimation, k_{21}, as a consequence of high CO concentration in the product gas unaccounted for by the thermodynamic equilibrium of the gas phase reactions.

4.2. Gas phase analysis

The gasification model will primarily be used to discuss the gas phase analysis; however results from both models will be presented and compared. Gas composition vs. residence time data for supercritical water gasification of 4.0 wt% (0.28 M) aqueous solution of xylose at 450 °C, 500 °C, 550 °C, and 650 °C are presented in Fig. 7(A) for the decomposition kinetic model and Fig. 7(B) for the gasification kinetic model. The solid and dashed lines represent model predictions. Major gas products at all conditions tested were H_2 and CO_2, and minor gas products were CH_4, CO, and C_2H_6. Small amounts (< 0.5%) of ethane and acetylene were identified but not quantified.

At 650 °C, gas composition (62% ± 1.3% H_2, 33.7% ± 0.9% CO_2, 2.6% ± 0.6% CH_4, 1.6% ± 1.3% CO, 0.2% ± 0.07% C_2H_6) was independent of residence time, and both models predicted gas compositions similar to experimental results. For reaction temperatures of 550 °C and lower, the majority of the product gas comprised of CO_2 and H_2, however, the product gas contained significant amount of CH_4 and CO. An increase in the concentration of CO was observed as reaction temperature and residence time were decreased. The high concentration of CO was not predicted by the decomposition or gasification kinetic models, and may affect the H_2 yield due to a lower than predicted CO conversion of the water gas shift reaction. Although the equilibrium constant for the water gas shift decreases as temperature decreases from 650 °C to 450 °C, the large excess of water in the feed drives the forward water gas shift reaction by the law of mass action. The highest predicted concentration of CO by the gasification model was 0.8% at 650 °C. Even though Ni and Cr rich alloys, such as Inconel and Hastelloy, drastically increase the reaction rate of the water gas shift [38], the higher than predicted concentration of CO at short residence times is likely due to non-equilibrium conversion of CO.

CH_4 in the product gas is produced from essentially two sources, gas phase reactions i.e. the methanation, and hydrogasification, and from reactions of organic liquid intermediates [39]. Since no coke or char formation was observed at any conditions tested, the hydrogasification reaction was not included in the reaction mechanism. At 650 °C the concentration of CH_4 in the product gas was independent of residence time, however, at reaction temperatures between 450 °C and 550 °C, the concentration CH_4 increased with residence time and eventually approached a constant value between 4% and 7%. The gasification kinetic model predicts significant amounts of CH_4 in the product gas and is in good agreement with experimental results, whereas the decomposition kinetic model does not predict any CH_4. Since both models assume thermodynamic equilibrium, the difference is attributed to non-ideal interactions accounted for in the gasification kinetic model. Fugacity coefficients for all of the gas phase species deviated from unity. Previous studies on the thermodynamic analysis for the supercritical water gasification of glucose have also predicted significant amounts of methane at similar reaction conditions [37,40].

The effect of reactor residence time on carbon gasification efficiency (CGE) and H_2 yield is presented in Fig. 8. The dashed lines represent the decomposition kinetic model predictions and the solid lines represent the gasification kinetic model. In general carbon gasification efficiency increased with residence time and reaction temperature. CGE model predictions from both models fit the experimental data well. As expected the gasification kinetic model more accurately predicts CGE at higher reaction temperatures whereas the decomposition kinetic model better predicts CGE at lower temperatures where gasification is not dominant.

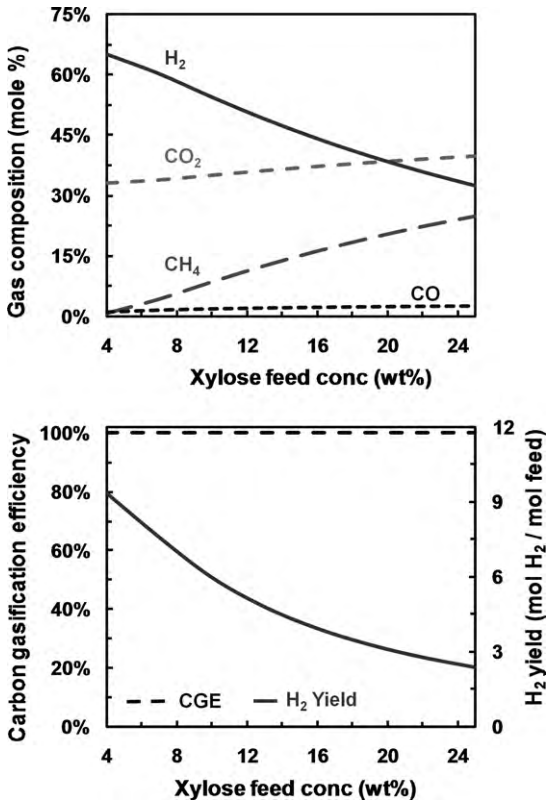

Fig. 9. Predicted gas composition (A), carbon gasification efficiency, and H_2 yield (B) as a function of feed concentration. The predictions were from the gasification kinetic model at 650 °C, 250 bar and a 10 s average fluid residence time.

The hydrogen yield, defined as moles of H_2 generated per mole of xylose fed, increased with reaction temperature and residence time. At 650 °C near stoichiometric H_2 yields for reforming, 8.9 ± 0.5 was achieved for fluid residence times of 0.9–4.7 s. The H_2 yield based on xylose reforming is

$$C_5H_{10}O_5 + 5H_2O \rightarrow 5CO_2 + 10H_2 \quad (56)$$

Theoretically it is possible to produce 10 mol of H_2 per mole of xylose reacted. H_2 yield model predictions from the gasification model tended to fit the experimental data well, whereas the decomposition kinetic model over predicted the H_2 yield as a result of under predicting the methane in the product gas. Hydrogen yields approaching 5 mol of H_2, the theoretical hydrogen yield based solely on the hydrogen in xylose, were reached at a reaction temperature of 500 °C and a fluid average residence time of 25 s.

4.3. High feed concentration analysis

The gasification kinetic model was used to predict gas composition and H_2 yield at 650 °C, 250 bar, and 10.0 s residence time from concentrated feed solutions. This model assumes that all the reactions are first order or pseudo first order, and the carbon gasification efficiency was 100%. The analysis is essentially used to investigate the effect of feed concentration on the thermodynamic equilibrium of the gas composition due to the water gas shift and methanation reactions.

Carbon gasification efficiency and H_2 yield are presented in Fig. 9. The predicted H_2 yield decreased from 9.4 mol of H_2 produced per mole of xylose reacted with a 4.0 wt% feed solution concentration to 2.4 mol of H_2 produced per mole of xylose reacted with a 25 wt% feed solution concentration. The decrease in H_2 yield is due to changes in the equilibrium gas composition rather than incomplete CGE. Gas composition as a function of feed solution concentration is presented in Fig. 9. As feed concentration increases, the concentration of CH_4 in the gas products increases. This is likely due to a decrease in the concentration of water as a result of water being consumed by the water gas shift reaction as well as an increase in the H_2 concentration relative to the concentration of water.

5. Conclusion

Two kinetic models that describe supercritical water gasification of xylose were proposed. Rate constants for both models were non-linearly estimated from product yield vs. residence time data. The decomposition model kinetically describes the how xylose is broken down to liquid intermediates, and is relevant to analysis of low temperature supercritical water gasification of hemicellulose, or for production of chemicals from xylose. The gasification kinetic model assumes all gas phase reactions are in thermodynamic equilibrium and uses a simplified reaction mechanism to model gasification rates and gas composition. The gasification kinetic model is ideal for optimizing supercritical water gasification of hemicellulose at conditions where gasification is dominant. Additionally, the gasification model is used to predict gas composition and H_2 yield as a function of feed concentration.

Acknowledgements

This research was supported by Bend Research, Inc., Bend, OR, and by the US Army under the Tactical Energy Systems program administered through the Oregon Nanoscience and Microtechnologies Breakthrough Institute.

References

[1] B. Saha, Hemicellulose bioconversion, Journal of Industrial Microbiology & Biotechnology 30 (2003) 279–291.
[2] N. Mosier, C. Wyman, B. Dale, R. Elander, Y. Lee, M. Holtzapple, M. Ladisch, Features of promising technologies for pretreatment of lignocellulosic biomass, Bioresource Technology 96 (2005) 673–686.
[3] A. Hendriks, G. Zeeman, Pretreatments to enhance the digestibility of lignocellulosic, Biomass Bioresource Technology 100 (2009) 10–18.
[4] A. Goodwin, G. Rorrer, Conversion of xylose and xylose–phenol mixtures to hydrogen-rich gas by supercritical water in an isothermal microtube flow reactor, Energy and Fuels 23 (2009) 3818–3825.
[5] F.K. Agbogbo, G. Coward-Kelly, Cellulosic ethanol production using the naturally occurring xylose-fermenting yeast, *Pichia stipitis*, Biotechnology Letters 30 (2008) 1515–1524.
[6] Y. Matsumura, T. Minowa, B. Potic, S. Kersten, W. Prins, W. van Swaaij, B. Beld, D. Elliott, G. Neuenschwander, A. Kruse, M. Antal, Biomass gasification in near- and super-critical water: status and prospects, Biomass and Bioenergy 29 (2005) 269–292.
[7] Y. Calzavara, C. Joussot-Dubien, G. Boissonnet, S. Sarrade, Evaluation of biomass gasification in supercritical water process for hydrogen production, Energy Conversion and Management 46 (2005) 615–631.
[8] A. Loppinet-Serani, C. Aymonier, F. Cansell, Current and foreseeable applications of supercritical water for energy and the environment, ChemSusChem 1 (2008) 486–503.
[9] R.M. Navarro, M.C. Sánchez-Sánchez, M.C. Alvarez-Galvan, F. del Valle, J.L.G. Fierro, Hydrogen production from renewable sources: biomass and photocatalytic, Energy and Environmental Science 2 (2009) 35–54.
[10] A.A. Peterson, F. Vogel, R.P. Lachance, M. Fröling, M.J. Antal Jr., J. Tester, Thermochemical biofuel production in hydrothermal media: a review of sub- and supercritical water technologies, Energy and Environmental Science 1 (2008) 32–65.
[11] A. Kruse, Supercritical water gasification, Biofuels Bioproducts & Biorefining 2 (2008) 415–437.
[12] T. Yoshida, Y. Matsumura, Gasification of cellulose, xylan, and lignin mixtures in supercritical water, Industrial and Engineering Chemistry Research 40 (2001) 5469–5474.
[13] A. Goodwin, G. Rorrer, Conversion of glucose to hydrogen-rich gas by supercritical water in a microchannel reactor, Industrial and Engineering Chemistry Research 47 (2008) 4106–4114.
[14] R.H. Holgate, J.C. Meyer, J.W. Tester, Glucose hydrolysis and oxidation in supercritical water, AIChE Journal 41 (1995) 637–647.
[15] X. Hao, L. Guo, X. Mao, X. Zhang, X. Chen, Hydrogen production from glucose used as a model compound of biomass gasified in supercritical water, International Journal of Hydrogen Energy 28 (2003) 55–64.

[16] S.R.A. Kersten, B. Potic, W. Prins, W.P.M. Van Swaaij, Gasification of model compounds and wood in hot compressed water, Industrial and Engineering Chemistry Research 45 (2006) 4169–4177.
[17] D. Yu, M. Aihara, J.A.J. Antal, Hydrogen production by steam reforming glucose in supercritical water, Energy and Fuels 7 (1993) 574–577.
[18] K. Ehara, S. Saka, A comparative study on chemical conversion of cellulose between the batch type and flow type systems in supercritical water, Cellulose 9 (2002) 301–311.
[19] F.L.P. Resende, M.E. Neff, P. Savage, Noncatalytic gasification of cellulose in supercritical water, Energy and Fuels 21 (2007) 3637–3643.
[20] P. Williams, J. Onwudili, Subcritical and supercritical water gasification of cellulose, starch, glucose, and biomass waste, Energy & Fuels 20 (2006) 1259–1265.
[21] Y Matsumura, S. Yanachi, T. Yoshida, Glucose decomposition kinetics in water at 25 MPa in the temperature range of 448–673 K, Industrial and Engineering Chemistry Research 45 (2006) 1875–1879.
[22] T. Yoshida, Y. Oshima, Y. Matsumura, Gasification of biomass model compounds and real biomass in supercritical water, Biomass and Bioenergy 26 (2004) 71–78.
[23] Y. Ogihara, R. Smith, H. Inomata, K. Arai, Reaction of cellulose–starch gel mixtures in water at high-temperatures and pressures for developing continuous batch microreactor systems, Cellulose 12 (2005) 595–606.
[24] Y.J. Lu, L.J. Guo, C. Ji, X. Zhang, X. Hao, Q. Yan, Hydrogen production by biomass gasification in supercritical water: a parametric study, International Journal of Hydrogen Energy 31 (2006) 822–831.
[25] T. Yoshida, Y. Matsumura, Reactor development for supercritical water gasification of 4.9 wt% glucose solution at 673 K by using computational fluid dynamics, Industrial and Engineering Chemistry Research 48 (2009) 8381–8386.
[26] F. Resende, P. Savage, Expanded and updated results for supercritical water gasification of cellulose and lignin in metal-free reactors, Energy and Fuels 23 (2009) 6213–6221.
[27] T. Yoshida, Y. Oshima, Partial oxidative and catalytic biomass gasification in supercritical water: a promising flow reactor system, Industrial and Engineering Chemistry Research 43 (2004) 4097–4104.
[28] M. Watanabe, Y. Aizawa, T. Iida, C. Levy, T.M. Aida, H. Inomata, Glucose reactions within the heating period and the effect of heating rate on the reactions in hot compressed water, Carbohydrate Research 340 (2005) 1931–1939.
[29] I.G. Lee, M.S. Kim, S.K. Ihm, Gasification of glucose in supercritical water, Industrial and Engineering Chemistry Research 41 (2002) 1182–1188.
[30] B.M. Kabyemela, T. Adschiri, R.M. Malaluan, K. Arai, Glucose and fructose decomposition in subcritical and supercritical water: detailed reaction pathway, mechanisms and kinetics, Industrial and Engineering Chemistry Research 38 (1999) 2888–2895.
[31] P. Williams, J. Onwudili, Composition of products from the supercritical water gasification of glucose: a model biomass compound, Industrial and Engineering Chemistry Research 44 (2005) 8739–8749.
[32] B.M. Kabyemela, T. Adschiri, R.M. Malaluan, K. Arai, Kinetics of glucose epimerization and decomposition in subcritical and supercritical water, Industrial and Engineering Chemistry Research 36 (1997) 1552–1558.
[33] A. Sinag, A. Kruse, J. Rathert, Influence of the heating rate and the type of catalyst on the formation of key intermediates and on the generation of gasses during hydropyrolysis of glucose in supercritical water in a batch reactor, Industrial and Engineering Chemistry Research 43 (2004) 502–508.
[34] L. Guo, Y. Lu, X. Zhang, C. Ji, Y. Guan, A. Pei, Hydrogen production by biomass gasification in supercritical water: a systematic experimental and analytical study, Catalysis Today 129 (2007) 275–286.
[35] J. Qi, L. Xiuyang, Kinetics of non-catalyzed decomposition of D-xylose in high temperature liquid water, Chinese Journal of Chemical Engineering 15 (2007) 666–669.
[36] M. Sasaki, T. Hayakawa, K. Arai, T. Adschiri, Hydrothermal reactions and techniques, in: Proceedings of the Seventh International Symposium on Hydrothermal Reactions 2, 2003, pp. 169–176.
[37] H. Tang, K. Kitagawa, Supercritical water gasification of biomass: thermodynamic analysis with direct Gibbs free energy minimization, Chemical Engineering Journal 106 (2005) 261–267.
[38] F. Bustamante, R.P. Enick, B.H. Killmeyer, K.S. Howard, Rothenberger, A.V. Cugini, B.D. Morreale, M.V. Ciocco, Uncatalyzed and wall-catalyzed forward water–gas shift reaction kinetics, AIChE Journal 51 (2005), 1540-1454.
[39] F. Resende, S. Fraley, M. Berger, P. Savage, Noncatalytic gasification of lignin in supercritical water, Energy and Fuels 22 (2008) 1328–1334.
[40] F.A.P. Voll, C.C.R.S. Rossi, C. Silva, R. Guirardello, R.O.M.A. Souza, V.F. Cabral, L. Cardozo-Filho, Thermodynamic analysis of supercritical water gasification of methanol, ethanol, glycerol, glucose and cellulose, International Journal of Hydrogen Energy 34 (2009) 9737–9744.